

Document downloaded from:

<http://hdl.handle.net/10251/165305>

This paper must be cited as:

Cerrillo, J.L.; Lopes, C.W.; Rey Garcia, F.; Agostini, G.; Kiwi-Minsker, L.; Palomares Gimeno, A.E. (2020). Nature and evolution of Pd catalysts supported on activated carbon fibers during the catalytic reduction of bromate in water. *Catalysis Science & Technology*. 10(11):3646-3653. <https://doi.org/10.1039/d0cy00606h>



The final publication is available at

<https://doi.org/10.1039/d0cy00606h>

Copyright The Royal Society of Chemistry

Additional Information

## ARTICLE

## Catalytic study and characterization of Pd supported on active carbon fibers for the reduction of bromate in water phase

Jose L. Cerrillo<sup>a</sup>, Christian W. Lopes<sup>a,b</sup>, Fernando Rey<sup>a</sup>, Giovanni Agostini<sup>c</sup>, Liubov Kiwi-Minsker<sup>d,e</sup>, Antonio E. Palomares<sup>a,\*</sup>

Received 00th January 20xx,  
Accepted 00th January 20xx

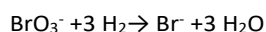
DOI: 10.1039/x0xx00000x

Catalytic hydrogenation of bromate using Pd catalysts supported on activated carbon fibers is a smart solution to treat bromate polluted water. These catalysts have been analyzed by different techniques for an in-deep characterization of the active sites. The *in-situ* X-ray absorption spectroscopy and the CO chemisorption studies showed that Pd<sup>0</sup> nanoparticles with different crystal sizes were generated on the support during hydrogen activation at 200 °C and that the PdH<sub>x</sub>-phase was formed during the cooling to room temperature. As PdH<sub>x</sub> species formed on Pd<sup>0</sup> nanoparticles are responsible for bromate reduction, the most active catalysts are those having Pd<sup>0</sup> nanoparticles with large crystal sizes, where PdH<sub>x</sub> species are easily formed. The catalysts are fully stable upon recycling during a number of reuses. It has been also shown that bromate reduction rate depends on the bromate concentration and on the hydrogen partial pressure, with a pseudo-first reaction order towards both reactants.

### Introduction

Bromate is a non-natural water pollutant<sup>1-3</sup> classified as mutagenic and carcinogenic for humans (Group 2B). For this reason, the World Health Organization has strictly limited bromate concentration in drinking water with a maximum of 10 ppb<sup>4</sup>.

Catalytic reduction of bromate to innocuous bromide, using hydrogen as reducing agent, is an effective technique that can be used for the removal of this pollutant according to:



Catalysts based on metallic palladium supported on different materials have been used for hydrogenation reactions<sup>5-10</sup> and may be used for the treatment of bromate polluted water<sup>11</sup>. Chen et al.<sup>12</sup> have studied different Pd and Pt catalysts for this reaction. They found that Al<sub>2</sub>O<sub>3</sub> is an appropriate support for these metals due to its high isoelectric point. Moreover, they described that Pd/Al<sub>2</sub>O<sub>3</sub> exhibited higher catalytic activity than Pt/Al<sub>2</sub>O<sub>3</sub>. Recently new publications reported the use of mono and bimetallic catalysts supported on zeolites<sup>13, 14</sup>, on active carbon<sup>15</sup>, carbon nanotubes<sup>16, 17</sup>, TiO<sub>2</sub><sup>16, 18</sup> or magnetite<sup>19</sup>. Moreover, platinum group metals as Rh, Ru and Ir supported on alumina or activated carbon, have been also proposed<sup>20</sup> as

catalysts for the reduction of aqueous oxyanion pollutants, including bromate, nitrate and/or perchlorate. The influence of the operation mode has been recently discussed for batch and continuous reactors<sup>20, 21, 22</sup>. It has been shown that Pd catalysts within structured reactors<sup>11, 23</sup> are a valuable option to treat natural and industrial wastewater polluted by bromate in continuous mode. Additionally, bimetallic Pd-Sn catalyst allows the simultaneous removal of bromate and nitrate from softly polluted water<sup>24-26</sup>. Recently new papers have appeared reporting the use of electrocatalysis<sup>27, 28</sup> and photocatalysis<sup>29, 30</sup> for the reduction of bromates.

Despite of the research on the bromate reduction reaction with Pd/catalysts, there is no any in-deep study characterizing the Pd species responsible for the activity in that reaction. Here, we have tried to characterize the nature and the evolution of a Pd catalyst supported on activated carbon fibers (ACF) during the hydrogenation of bromate in water at room temperature and atmospheric pressure. ACF have been selected as support due to their high specific surface area, their availability in diverse forms (powder, pellets, cloth, paper, mat, etc) offering many options for reactor designs and for their excellent mass and heat transfer characteristics, low pressure drop and ease handling<sup>5, 31-34</sup>. Pd supported ACF catalyst has shown a high activity for the catalytic reduction of bromates in water phase using a continuous reactor and with different polluted waters<sup>23-26, 35</sup>. In this work the Pd/ACF catalyst has been thoroughly characterized using powerful techniques such as *in-situ* X-ray absorption spectroscopy (XAS), CO chemisorption, XPS and field emission scanning electron microscopy (FESEM) coupled with an energy dispersive X-ray analysis (EDS) in order to determine the evolution of the active phase in the catalyst preparation and in the reaction media. These results have allowed establishing

<sup>a</sup> Instituto de Tecnología Química (CSIC - Universitat Politècnica de València), Camino Vera s.n., Valencia, 46022, Spain.

<sup>b</sup> CAPES, Ministério da Educação do Brasil, Brasília, 70040-020, Brazil.

<sup>c</sup> CELLS – ALBA Synchrotron Radiation Facility, Barcelona, Spain.

<sup>d</sup> Ecole Polytechnique Fédérale de Lausanne (EPFL), CH-1015, Switzerland

<sup>e</sup> Tver State University, 170100, Russian Federation

Electronic Supplementary Information (ESI) available.

See

DOI: 10.1039/x0xx00000x

the active sites main characteristics that are responsible for the catalyst activity.

## Experimental

### Preparation of catalysts

Woven active carbon fibers supplied by Kynol® were pre-treated by boiling in a 15% HNO<sub>3</sub> solution during 1 hour in order to clean the surface and to oxidize the carbon surface, introducing oxygen-containing functional groups<sup>36</sup>. Afterwards, fibers were rinsed with deionized water and dried at room temperature. The palladium was added *via* incipient wetness impregnation. Different aqueous solutions with a variety of concentrations of Pd(NH<sub>3</sub>)<sub>4</sub>(NO<sub>3</sub>)<sub>2</sub> were used to obtain 5%, 1%, 0.5% and 0.25wt.% of Pd in the final catalyst. After impregnation, the catalysts were air-dried at room temperature and activated in a flow of 10% H<sub>2</sub> in N<sub>2</sub> at 200 °C during 1 h.

### Characterization

Micromeritics ASAP 2420 was used to characterize the catalysts textural properties by N<sub>2</sub> adsorption. The BET surface area was determined by applying the method of Brunauer, Emmett and Teller fulfilling the criterion established by Rouquerol et al.<sup>37</sup>. Field emission scanning electron microscopy (FESEM) images of the catalysts were obtained with a ZEISS ULTRA 55 operating at 20 kV. This microscope was equipped with an energy dispersive X-ray system (EDS) for analysis and mapping of elements.

X-ray photoelectron spectroscopy (XPS) experiments were collected on a SPECS spectrometer with a Phoibos 150 MCD-9 detector using non-monochromatic MgK<sub>α</sub> (1253.6 eV) X-ray radiation. The pass energy was 20 eV with an operating pressure of 10<sup>-9</sup> mbar. During the data processing of the XPS spectra, bending energy values were referenced to the C1s peak (BE=284.5 eV). Spectral treatment was performed by using CASA software.

The average Pd metal crystallite diameter and its dispersion in the reduced samples were estimated from CO chemisorption with the double isotherm method using a Quantachrome Autosor-1C equipment. Prior to adsorption, the samples were reduced *in situ* by flowing hydrogen at 200 °C. After that they were degassed at 1333 Pa for 2 h and cooled down to 35 °C.

Then, pure CO was admitted and the first adsorption isotherm (i.e. the total CO uptake) was measured. After evacuation at 35 °C, the second isotherm (i.e. the reversible CO uptake) was obtained. The amount of chemisorbed CO was found by subtracting the two isotherms. The metal dispersion was calculated from the amount of irreversibly adsorbed CO assuming a Pd/CO atomic ratio of 1. The average Pd crystallite diameter was determined from chemisorption data assuming spherical geometry for the metal particles according to the procedure described by Anderson<sup>38,39</sup>.

X-ray absorption experiments, at the Pd (24350 eV) K-edge, were carried out at the BL22 (CLÉSS), beamline of ALBA synchrotron (Spain). The white beam was monochromatized using a Si (311) double crystal cooled by liquid nitrogen; harmonic rejection was performed using Rh-coated silicon mirrors. The spectra were collected in transmission mode by means of ionization chambers, filled with appropriate gases. Pd-based samples were packed into a stainless-steel sample holder and placed inside a multipurpose cell that allows *in situ* evacuation, multiple gas manipulation and modification of the temperature<sup>40</sup>. Several scans were acquired at each measurement to ensure spectral reproducibility and good signal-to-noise ratio. The XAS data analysis was performed using IFFEFIT package<sup>41</sup>. Phase and amplitudes were calculated by FEFF6 code and were successfully checked with Pd metal foil. For each sample, the averaged  $k^3\chi(k)$  function were Fourier transformed in a determined  $\Delta k = 2.3 - 12.8 \text{ \AA}^{-1}$  interval. The fits were performed in R-space in the  $\Delta R = 2.0 - 3.0 \text{ \AA}$  range, resulting in a number of independent points equal to 6.3. To reduce the correlation between the parameters, the fits were performed in different k-weights. Passive electron amplitude reduction factor was fixed to that found for metallic Pd ( $S_0^2 = 0.75$ ).

The evolution of the palladium species during the reaction was *in situ* monitored using the same multipurpose system described above but replacing that cell by another one adapted for solid-liquid-gas catalytic experiments<sup>40</sup>. In those experiments Pd-ACF were packed in a sample holder where the liquid reactant (50 ppm of BrO<sub>3</sub><sup>-</sup> previously hydrogenated) was flowed through the catalyst using a HPLC pump at room temperature and atmospheric pressure.

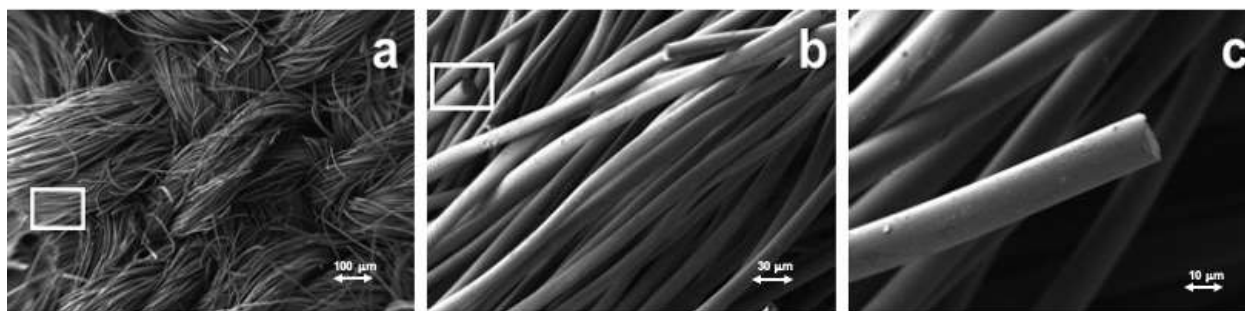


Figure 1: FESEM images of 1 wt.% Pd /ACF at different magnifications (from a to c: x38, x350, x 1000)

### Catalytic activity

The catalytic activity was tested in a 1 L batch reactor, stirred at 900 rpm with a mechanical Teflon stirrer. The bromate solutions were prepared from NaBrO<sub>3</sub> and the reactions were run at room temperature and atmospheric pressure using a constant volume of 0.6 L with 50 ppm of bromate. In some experiments the bromate concentration was modified (50, 100 and 150 ppm) keeping constant the other conditions. The mass of the catalyst was 0.5 g in each run. Before the reaction, the solution was bubbled with pure hydrogen (250 mL·min<sup>-1</sup>) through a diffuser during 2 h in order to saturate the solution by hydrogen and to remove the solved oxygen. The same hydrogen flow was maintained during the reaction. In some experiments, the partial pressure of hydrogen was modified by substituting part of the hydrogen by nitrogen but keeping the total gas flow rate constant.

For assessing catalyst stability, the used catalyst was filtered after the reaction, dried at 100 °C and reused again in a new reaction run. In all the experiments aliquots of the reaction mixture were taken at different times for monitoring the reaction progress. Bromate and bromide were analyzed with ionic chromatograph 883 Basic IC Plus (Metrohm®) equipped with a conductivity detector and a chemical suppressor. The anions were separated using a Metrosep-A Supp-5 150/4 column and a Metrosep-A Supp 5 150/4 pre-column. The operating conditions as injection volume, flow rate and temperature were set at 20 µL, 0.7 mL·min<sup>-1</sup> and 22 °C. The eluent was a solution of 3.2 mM Na<sub>2</sub>CO<sub>3</sub> and 1.0 mM NaHCO<sub>3</sub>, with 50 mM H<sub>2</sub>SO<sub>4</sub> solution used as chemical suppressor. The conversion was calculated as mols of reacted bromate referred to the mols of initial bromate. The TOF was calculated as the initial reaction rate (at bromate conversions below 30%) divided by the mols of exposed Pd. The mols of exposed Pd were calculated with the data of Pd content (measured by EDS) and Pd dispersion (obtained by CO chemisorption).

Inductively coupled plasma (ICP-OES) in a Varian 715-ES ICP-Optical Emission Spectrometer was used to determine the possible leaching of Pd from the support to the reaction media.

of micropores and some mesoporosity. Table 1 shows the textural properties of the catalysts. It can be observed that all the materials had a very high surface area with low mesoporous area, indicating that Pd/ACF were mostly microporous materials. The increase of Pd content on the support resulted in a slight decrease of the BET surface area, but the general textural properties did not change after Pd deposition. The palladium contents in all the catalysts, determined by EDS, were similar to the theoretical ones and showed a homogeneous distribution across the samples, indicating that the impregnation method used for the metal incorporation was adequate.

The physical structure and morphology of the catalysts were studied by FESEM. The micrograph of the ACF cloth (see supporting material, Figure S1) showed a plain weave pattern of carbon textile where fibers alternate up and down. The addition of Pd to the ACF (Figure 1) did not change the macroscopic structure of the fibers, neither the fiber morphology with a diameter of 10-12 microns.

X-ray absorption spectroscopy, in both XANES and EXAFS regions, was applied to characterize the evolution of a Pd/ACF catalyst during its preparation, this is i) after ACF impregnation of the Pd precursor (O<sub>2</sub>-25 °C), ii) after activation in flow of H<sub>2</sub> at room temperature (H<sub>2</sub>-25 °C) and at 200 °C (H<sub>2</sub>-200 °C), and iii) after cooling the sample down to room temperature (H<sub>2</sub>-25 °C cooled). The normalized XANES spectra are shown in Figure 2 (left) and compared to those of bulk Pd(NO<sub>3</sub>)<sub>2</sub> and Pd foil, references for Pd<sup>2+</sup> and for Pd<sup>0</sup> species. The spectrum at room temperature after the impregnation, presented similar features to the Pd(NO<sub>3</sub>)<sub>2</sub> standard, with the absorption edge positioned at 24354 eV, characteristic of palladium 2+. Introduction of hydrogen at room temperature did not change the spectrum, maintaining the same features. However, increasing the temperature up to 200 °C in the presence of hydrogen resulted in an absorption edge shift to lower energy (24350 eV), indicating a reduction of Pd<sup>2+</sup> species to Pd<sup>0</sup>. The change in edge position was accompanied by the appearance of well-defined EXAFS oscillations immediately after the edge (negative and positive peaks at 24382 and 24397 eV, respectively). These strong features were due to the well-arranged local *fcc* structure of Pd<sup>0</sup>, where 12 Pd atoms are coordinated at the same distance from the central Pd atom<sup>42, 43</sup>. The intensity of these features contains intrinsic information on the Pd particle size, which could serve to discriminate between bulk Pd and nanosized Pd species. In this way, it was observed that the spectrum at 200 °C was flattened as compared to the Pd<sup>0</sup>-foil standard, indicating the formation of Pd nanoparticles and not bulk Pd<sup>43</sup>. After cooling down to room temperature under hydrogen, no changes in the oscillation intensities were observed, which indicates that no further aggregation of Pd nanoparticles took place. However, the oscillations beyond edge were slightly shifted to lower energies in respect to the spectrum of Pd metal foil, which could be attributed to the formation of PdH<sub>x</sub>-like phase not stable at high temperatures<sup>44, 45</sup>. Features in the pre-edge region were not observed in any spectra suggesting centrosymmetric geometry around

Table 1: Catalysts textural properties and Pd content (measured by EDS)

	Pd content (wt %)	BET area (m <sup>2</sup> /g)	Microporous area (m <sub>2</sub> /g)
ACF	-	1977	1928
0.25%Pd/ACF	0.22	1885	1837
0.5% Pd/ACF	0.48	1848	1801
1% Pd/ACF	0.96	1812	1767
5% Pd/ACF	4.81	1653	1605

## Results & Discussion

### Characterization of materials

The Pd/ACF textural properties were studied by N<sub>2</sub> adsorption at -196 °C showing a Ib type isotherm, suggesting the presence

palladium atoms at all the temperatures and atmospheres studied<sup>46</sup>.

The  $k^3$ -weighted, phase-uncorrected  $\chi(k)$  functions related to the reduction step of the catalyst are shown in Figure S2-a and compared to those of bulk  $\text{Pd}(\text{NO}_3)_2$ , used as reference for  $\text{Pd}^{2+}$ , and to those of Pd foil, used as reference for  $\text{Pd}^0$  species. The spectra oscillations recorded at 25 °C in  $\text{O}_2$  and  $\text{H}_2$  closely resembled those of  $\text{Pd}(\text{NO}_3)_2$  spectrum. In contrast, the EXAFS signals of the sample measured in  $\text{H}_2$  at 200 °C matched perfectly with the signal of metallic  $\text{Pd}^0$ , although the intensities of these oscillations were flattened as compared with those of Pd foil, suggesting the nanosized character of the formed species<sup>47</sup>. Cooling the sample down to 25 °C under  $\text{H}_2$  resulted in a shift to smaller values of  $k$ -space (light blue line), which suggested an increase of Pd-Pd distances in the metal nanoparticles due the insertion of H atoms in Pd lattice forming  $\text{PdH}_x$ . The  $k^3$ -weighted EXAFS data were Fourier transformed and the results are shown in Figure S2-b. The FT spectrum showed two peaks at different stages. The first one between 1-2 Å (not corrected in phase) was related to the contribution Pd-O from the  $\text{Pd}(\text{NO}_3)_2$  used as Pd precursor. This peak remained when  $\text{O}_2$  was changed by  $\text{H}_2$  at room temperature. The second one, positioned between 2-3 Å, was attributed to Pd-Pd contribution from  $\text{Pd}^0$  nanoparticles and appeared after reduction at 200 °C. The spectrum of the reduced sample differed significantly in respect to that of Pd foil, which indicates the formation of Pd nanoparticles instead of palladium bulk. Also, it was possible to observe the difference in phase after cooling in hydrogen, due the  $\text{PdH}_x$  species formation.

The quantitative results obtained from the EXAFS data analysis of Pd foil and reduced Pd/ACF are shown in Table 2. For Pd metal foil, the characteristic coordination number of 12, typical of noble metals arranged in *fcc* local structure with Pd-Pd distance of 2.74 Å was obtained. Besides, the Pd foil showed a Debye-Waller factor typical of well-ordered metals<sup>43</sup>. For the Pd catalyst analyzed at 200 °C in  $\text{H}_2$ , an average coordination number of 8.7 for Pd-Pd contribution was obtained, with a Pd-Pd distance of 2.73 Å, slightly shorter than Pd foil, confirming the formation of metal nanoparticles<sup>43</sup>. On the other hand, when the temperature was decreased to 25 °C, only a small increase in the average coordination number was observed, whilst a notable increment in the Pd-Pd bond distance appeared (2.80 Å), which is the consequence of hydride insertion in the

Pd nanoparticles yielding to  $\text{PdH}_x$  species, as previously stated<sup>45, 48</sup>. The Debye-Waller factors for the sample measured at 200 °C and cooled down were 0.0092 and 0.0072 Å<sup>2</sup> respectively, due to the thermal effect. However, a Debye-Waller factor equal to 0.0072 Å<sup>2</sup> can be also related to the static disorder intrinsic of formed nanoparticle<sup>49</sup>. Furthermore, all fits exhibited significantly low errors, confirming the quality of the fits (best-fits of catalysts during reduction at 200 °C and after reduction are reported in SI, Figure S3).

The stability of the Pd nanoparticles formed after activation and their evolution during the reaction was studied by measuring the XANES spectra under reaction conditions using a specially designed *in situ* cell. In these experiments the activated 5%Pd/ACF catalyst was packed in the sample holder and the water reactant (50 ppm of  $\text{BrO}_3^-$  solution previously saturated by hydrogen) was flowed through the catalyst while the XANES spectra were taken. It was verified that under these reaction conditions and with this catalyst, a 100% conversion of bromates to bromides was achieved. To the best of our knowledge, this is the first time that this type of study has been made for this liquid-solid reaction. The normalized XANES spectra (Figure 2 - right) of the catalyst in contact with the reaction feed, taken during the reaction, completely overlapped and were coincident with that obtained after activation under hydrogen at 200 °C and cooling the sample to room temperature. This indicates that the oxidation state of Pd and the nature of the formed nanoparticles were maintained during the catalytic reaction. Also, these results show that the bromates present in the reaction media did not oxidize the  $\text{Pd}^0$  nanoparticles maintaining the palladium hydride phase also intact.

*Ex situ* XPS studies were carried out with different catalysts. The spectra were very similar for all the materials, showing the characteristics  $3d_{3/2}$  and  $3d_{5/2}$  Pd peaks (Figure 3). The deconvolution of the Pd  $3d_{5/2}$  peaks demonstrates a similar distribution of the surface Pd in the catalysts. Palladium sites were mainly present as  $\text{Pd}^0$  (85% for the 1% Pd catalyst and 89% for the 0.5% Pd catalyst) although some (15% for the 1% Pd catalyst and 11% for the 0.5% Pd catalyst) positively charged  $\text{Pd}^{2+}$  was present in the catalyst. Similar results have been obtained with Pd catalysts used for the nitrate catalytic reduction<sup>50</sup>. The existence of oxidized Pd on the surface of the

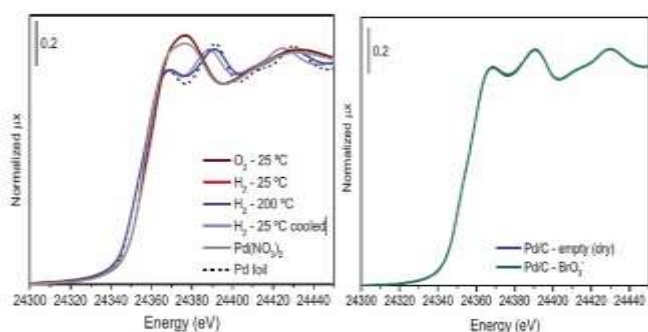


Figure 2: Normalized XANES spectra of 5% Pd/ACF and Pd-references during preparation of the catalyst (left) and during catalytic reduction of bromates in water (right)

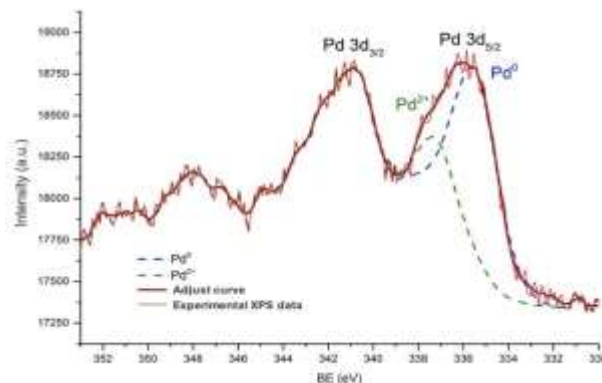


Figure 3: XPS spectra of the reduced 1%Pd/ACF catalyst

catalysts could be related with the presence of some  $\beta$ -PdH<sub>2</sub> species as suggested by the XANES study.

Table 2: Summary of the parameter optimized by fitting the EXAFS data of Pd foil and Pd/ACF<sup>‡</sup>

	Pd foil	Pd/ACF 200 °C (H <sub>2</sub> )	Pd/ACF 25 °C cooled (H <sub>2</sub> )
CN	12	8.7 ± 0.3	9.3 ± 0.4
S <sub>0</sub> <sup>2</sup>	0.75	-	-
R <sub>Pd-Pd</sub> (Å)	2.743 ± 0.003	2.729 ± 0.002	2.807 ± 0.003
σ <sup>2</sup> (Å <sup>2</sup> )	0.0053 ± 0.0005	0.0092 ± 0.0003	0.0072 ± 0.0004
ΔE <sub>0</sub> (eV)	4.3 ± 0.8	1.8 ± 0.3	2.4 ± 0.4
R-factor	0.0013	0.0007	0.0014

Table 3: Reaction rate, Pd content and dispersion, average particle size and TOF (0.6L, 0.5 g catalyst, RT, atmospheric pressure, 50 ppm BrO<sub>3</sub><sup>-</sup>)

	Reaction rate (converted BrO <sub>3</sub> <sup>-</sup> mmol /s)	Pd content (wt %)	Pd dispersion (%)	Average particle size (nm)	TOF (min <sup>-1</sup> )
0.25%Pd/ACF	2.11·10 <sup>-5</sup>	0.22	32.7	3.4	0.37
0.5%Pd/ACF	4.52·10 <sup>-5</sup>	0.48	19.7	5.5	0.61
1%Pd/ACF	9.22·10 <sup>-5</sup>	0.96	12.8	7.3	0.96

The dispersion of metallic Pd was calculated using CO chemisorption isotherms at 35 °C. These data are presented in Table 3, showing an increase of the metal dispersion and a decrease of the average particle size when Pd content decreases. The highest metallic dispersion and the smaller particle size were obtained with the 0.25 wt.% Pd/ACF catalyst and the lowest dispersion and the larger particle size were observed for the 1 wt.% Pd/ACF. A very similar trend was observed by a TEM analysis of the samples.

### Catalytic results

A blank reaction was performed without any catalyst. The results (not shown) prove that in the absence of catalyst, at room temperature and atmospheric pressure, bromates did not react significantly with hydrogen. The activity of the ACF support without Pd was also tested (Figure 4) observing a small conversion about 10%. Similar results have been previously reported for this reaction when using different activated carbon materials as catalytic supports<sup>22, 51, 52</sup>, and it was proposed<sup>53</sup> that bromates were reduced by the -C sites of the activated carbon surface, forming CO<sub>2</sub> and bromide. This mechanism could be responsible for the low conversion observed when ACF without Pd was used. Similar results were obtained with the non-activated catalyst showing that the Pd species present in the catalyst before the hydrogen thermal treatment are not active for this reaction. X-ray absorption experiments have shown that before activation, Pd was present as Pd<sup>2+</sup> and it remained in this oxidation state even in the presence of hydrogen at room temperature. This is clear evidence that Pd<sup>2+</sup> species cannot catalyze the reaction.

On the other hand, after catalyst activation by hydrogen at 200 °C, bromates are reduced to bromides at room temperature and atmospheric pressure. X-ray absorption characterization of the

material has shown that after activation, nanoparticles of metallic Pd<sup>0</sup> are formed. They remained stable after cooling to room temperature and contain some species of PdH<sub>x</sub>-phase. So, it can be stated that Pd<sup>0</sup> nanoparticles with PdH<sub>x</sub> species are the active phase responsible for the catalytic hydrogenation of bromates in water.

In order to evaluate the influence of the Pd nanoparticles size in the activity of the Pd/ACF, catalysts with different Pd contents resulting in different particle sizes, were evaluated under the same conditions (Figure 5) and the intrinsic activities of these catalysts (TOF) were calculated as the initial reaction rate referred to the accessible Pd sites. The amount of accessible Pd sites (those available for the reaction) was obtained multiplying the Pd content (EDS) by its dispersion (CO chemisorption) and the values obtained are shown in Table 3. It can be observed

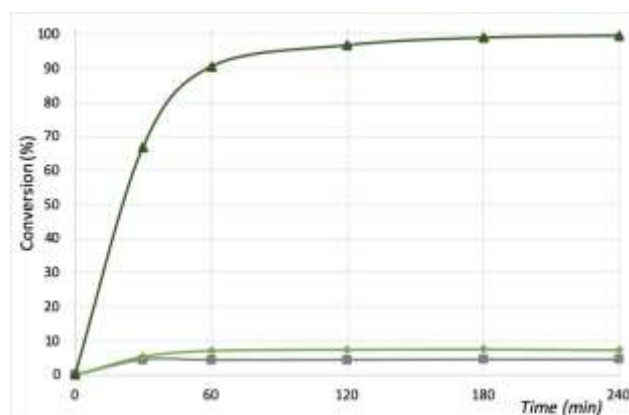


Figure 4: Catalytic activity of the support (ACF) (■), 1 wt.%Pd/ACF catalyst before activation (◆) same catalyst after activation with H<sub>2</sub> (▲), (0.6 L, 50 ppm of BrO<sub>3</sub><sup>-</sup>, 0.5 g catalyst, RT, atmospheric pressure).

that the intrinsic activity normalized to the Pd content increases with the amount of Pd in the catalyst. Nevertheless, the CO chemisorption analyses have shown that Pd dispersion decreases when increasing the metal content, forming Pd nanoparticles with larger crystal size. Then, the best activity per mol of Pd was obtained with catalysts with larger crystal size. It has been described that Pd nanoparticles with high diameter favor H<sub>2</sub> activation because make easy the dissociative adsorption of H<sub>2</sub> molecules, forming  $\beta$ -PdH surface species<sup>54</sup>. These species are the responsible for the bromate reduction as it was observed in the *in situ* XAS experiments.

The easiest formation of PdH<sub>x</sub> surface species on the catalyst with the larger crystal size, this is with the lowest metal dispersion, explains the highest activity, normalized to the Pd content, obtained with the catalysts with higher amount of palladium.

It must be pointed out that in all the reactions the amount of reacted bromates and produced bromides were the same, with 100% selectivity to the desired product. These results confirm the absence of stable intermediates or by-products.

The influence of bromate concentration and H<sub>2</sub> partial pressure on the catalytic reaction rate was studied. The evolution on time of the converted bromates when using different bromate initial concentrations (50, 100, 150 mg·L<sup>-1</sup>), while keeping constant the partial pressure of H<sub>2</sub>, are shown in Figure 6. It is observed that the initial reaction rates (mols of bromate converted per second at low conversion time) increase linearly with the bromate initial concentration. Similar experiments were performed modifying the partial pressure of H<sub>2</sub> (1, 0.5, 0.25) and maintaining constant the initial bromate concentration. The catalytic results (Figure 7) also reveal a direct dependence of the initial reaction rate on the partial pressure of H<sub>2</sub>. In the supporting information (Figure S4 and S5) reaction rates, expressed as mmols of converted bromates per second at low conversion time, are plotted against initial bromate concentration and against hydrogen partial pressure. A linear correlation is obtained in both cases with R<sup>2</sup> coefficients close to one and with the line passing through the origin. These results indicate a pseudo-first order reaction with respect both reagents, bromate and hydrogen. Previous studies have also

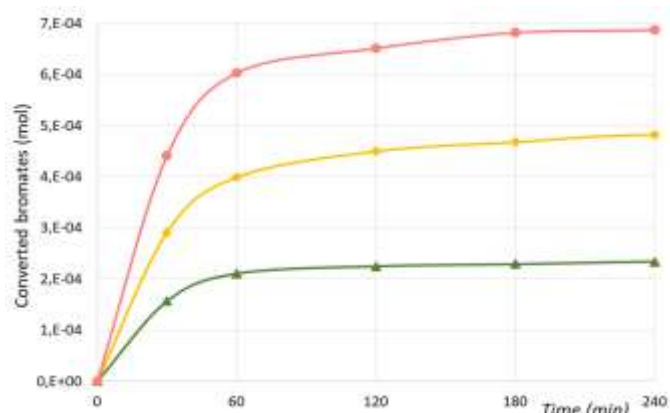


Figure 6: Converted bromates when using different bromate initial concentrations: 0.39 mmol/L ( $\blacktriangle$ ), 0.78 mmol/L ( $\blacklozenge$ ), 1.17 mmol/L ( $\bullet$ ), (0.6 L, 0.5 g of 1wt.%Pd/ACF catalyst, RT, atmospheric pressure).

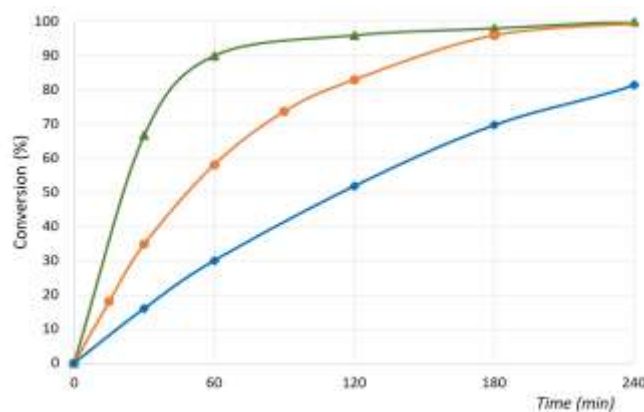


Figure 5: Catalytic activity of ACF with different Pd content (i.e. different particle size): 1wt.% ( $\blacktriangle$ ), 0.5wt.% ( $\bullet$ ) and 0.25wt.% ( $\blacklozenge$ ), (0.6 L, 50 ppm of BrO<sub>3</sub><sup>-</sup>, 0.5 g catalyst, RT, atmospheric pressure)

reported this kinetic behavior towards bromate concentration<sup>12, 21, 55</sup>, but no one had addressed the influence of the H<sub>2</sub> partial pressure. Here, we show that the reaction has a pseudo-first order in respect both reactants.

The stability of the catalyst was studied with the same catalyst in successive reaction runs and no deactivation was observed after three cycles of reaction as can be seen in the Supporting Information at Figure S6.

This permanence of the active species was also confirmed by the *in situ* X-ray absorption experiments made under reaction conditions as previously discussed. These results showed that the same oxidation state of Pd species and the same EXAFS oscillation features were obtained in the used catalysts and were maintained during the reaction. From the point of view of the morphology, the diameter of individual fibers was not modified after reaction with an approximate value of 10-12  $\mu$ m, neither the chemical composition of the catalyst, which was the same than before reaction, showing the stability of the material. Finally, the absence of palladium in the water solution after the successive runs also confirms that there is no leaching of the

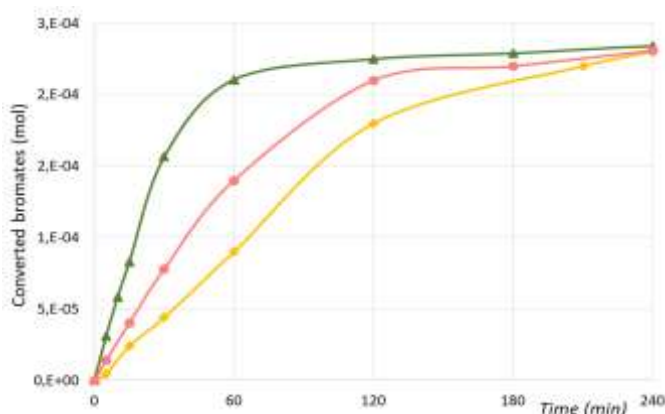


Figure 7: Converted bromates at different hydrogen partial pressure: 1 atm ( $\blacktriangle$ ), 0.5 atm ( $\bullet$ ), 0.25 atm ( $\blacklozenge$ ), (0.6 L, 0.39 mmol/L of BrO<sub>3</sub><sup>-</sup>, 0.5 g of 1wt.%Pd/ACF catalyst, RT, atmospheric pressure).

metal from the catalyst during reaction. This was confirmed by removing the Pd/ACF from the reaction media at half conversion and no further activity was observed.

## Conclusions

Pd supported on activated carbon fibers (ACF) is an effective catalyst for the complete and selective reduction of bromates in water by hydrogen to non-toxic bromide anions. The X-ray absorption spectroscopy studies have shown that Pd<sup>0</sup> nanoparticles are generated on the ACF support during the catalyst activation in hydrogen flow at 200 °C and that PdH<sub>x</sub> like-phase is formed when cooling down the catalyst with hydrogen to room temperature. The *in situ* XAS study of Pd/ACF catalyst under real reaction conditions confirms that Pd/PdH<sub>x</sub> supported on ACF remains unchanged during the reaction process, being the active phases for the bromate reduction. The palladium hydride species are more easily formed in Pd nanoparticles with large crystal size therefore, the normalized TOF activity (expressed per mol of Pd) increases as the palladium content does; i.e. when diminishes the metal dispersion. Pd/ACF can be reused in successive reaction runs without noticeable loss of activity proving the high stability of the Pd active species. Finally, a preliminary kinetic study of bromate reduction suggests a pseudo-first order towards concentration of bromate and hydrogen.

## Conflicts of interest

There are no conflicts to declare.

## Acknowledgements

Authors thank the Spanish Ministry of Economy and Competitiveness through RTI2018-101784-B-I00 (MINECO/FEDER) and SEV-2016-0683 projects for the financial support. We gratefully acknowledge ALBA synchrotron for allocating beamtime (proposal 2015091414) and CLÆSS beamline staff for their technical support during our experiment. C.W. Lopes (Science without Frontiers - Process no. 13191/13-6) thanks CAPES for a predoctoral fellowship. J.L. Cerrillo is grateful to MINECO for the Severo Ochoa contract for PhD formation (SVP-2014-068600). L. Kiwi-Minsker acknowledges financial support provided by Russian Science Foundation (project 15-19-20023). Authors also thank Kynol Europa GmbH for the supply of the active carbon fibers.

## Notes and references

‡ The fits were performed on the first coordination sphere ( $\Delta R = 2.0\text{-}3.0$  Å) over FT of the  $k^1$ ,  $k^2$  and  $k^3$ -weighted  $\chi(k)$  functions performed in the  $\Delta k = 2.3\text{-}12.8$  Å<sup>-1</sup> interval, resulting into a number of independent parameters of  $2\Delta R\Delta k/\pi=6.3$ . Non optimized parameters are recognizable by the absence of the corresponding error bar.

1. M. Naushad, M. R. Khan, Z. A. Al Othman, F. Rodriguez-Reinoso, T. M. Turki and R. Ali, *Environmental Science and Pollution Research*, 2015, **22**, 15853-15865.
2. R. Butler, A. Godley, L. Lytton and E. Cartmell, *Crit. Rev. Environ. Sci. Technol.*, 2005, **35**, 193-217.
3. H. S. Weinberg, C. A. Delcomyn and V. Unnam, *Environmental science & technology*, 2003, **37**, 3104-3110.
4. OMS, *Bromate in Drinking-water - Guidelines for Drinking-water Quality*, WHO, 2005.
5. M. Jabłońska, A. Król, E. Kukulska-Zajac, K. Tarach, V. Girman, L. Chmielarz and K. Góra-Marek, *Applied Catalysis B: Environmental*, 2015, **166**, 353-365.
6. S. B. Pergher, R. M. Dallago, R. C. Veses, C. E. Gigola and I. M. Baibich, *Journal of Molecular Catalysis A: Chemical*, 2004, **209**, 107-115.
7. B. P. Chaplin, M. Reinhard, W. F. Schneider, C. Schuth, J. R. Shapley, T. J. Strathmann and C. J. Werth, *Environ. Sci. Technol.*, 2012, **46**, 3655-3670.
8. V. Höller, K. Rådevik, I. Yuranov, L. Kiwi-Minsker and A. Renken, *Applied Catalysis B: Environmental*, 2001, **32**, 143-150.
9. W.-J. Shen, Y. Ichihashi, H. Ando, M. Okumura, M. Haruta and Y. Matsumura, *Applied Catalysis A: General*, 2001, **217**, 165-172.
10. J. Hirayama and Y. Kamiya, *Catalysis Science & Technology*, 2018, **8**, 4985-4993.
11. A. Palomares, C. Franch, T. Yuranova, L. Kiwi-Minsker, E. García-Bordeje and S. Derrouiche, *Applied Catalysis B: Environmental*, 2014, **146**, 186-191.
12. H. Chen, Z. Xu, H. Wan, J. Zheng, D. Yin and S. Zheng, *Applied Catalysis, B: Environmental*, 2010, **96**, 307-313.
13. O. S. G. P. Soares, C. M. A. S. Freitas, A. M. Fonseca, J. J. M. Orfao, M. F. R. Pereira and I. C. Neves, *Chem. Eng. J.*, 2016, **291**, 199-205.
14. C. M. A. S. Freitas, O. S. G. P. Soares, J. J. M. Orfao, A. M. Fonseca, M. F. R. Pereira and I. C. Neves, *Green Chem.*, 2015, **17**, 4247-4254.
15. J. Restivo, O. S. G. P. Soares, J. J. M. Orfao and M. F. R. Pereira, *Catalysis Today*, 2015, **249**, 213-219.
16. J. Restivo, O. Soares, J. Orfao and M. Pereira, *Chemical Engineering Journal*, 2017, **309**, 197-205.
17. O. Soares, P. Ramalho, A. Fernandes, J. Órfão and M. Pereira, *Journal of Environmental Chemical Engineering*, 2019, **7**, 103015.
18. A. M. Perez-Coronado, O. S. G. Soares, L. Calvo, J. J. Rodriguez, M. A. Gilarranz and M. F. R. Pereira, *Applied Catalysis B: Environmental*, 2018, **237**, 206-213.
19. M. Li, X. Zhou, J. Sun, H. Fu, X. Qu, Z. Xu and S. Zheng, *Science of The Total Environment*, 2019, **663**, 673-685.
20. X. Chen, X. Huo, J. Liu, Y. Wang, C. J. Werth and T. J. Strathmann, *Chem. Eng. J.*, 2017, **313**, 745-752.
21. Y. Gao, W. Sun, W. Yang and Q. Li, *Scientific Reports*, 2017, **7**, 41797.
22. M. Li, Y. Hu, H. Fu, X. Qu, Z. Xu, S. Zheng, *Chem. Comm.*, 2019, **55**, 11786-11789.
23. Y. Marco, E. Garcia-Bordeje, C. Franch, A. E. Palomares, T. Yuranova and L. Kiwi-Minsker, *Chem. Eng. J.*, 2013, **230**, 605-611.
24. T. Yuranova, L. Kiwi-Minsker, C. Franch, A. E. Palomares, S. Armenise and E. Garcia-Bordeje, *Ind. Eng. Chem. Res.*, 2013, **52**, 13930-13937.
25. A. E. Palomares, C. Franch and A. Corma, *Catal. Today*, 2011, **172**, 90-94.
26. T. Yuranova, C. Franch, A. E. Palomares, E. Garcia-Bordeje and L. Kiwi-Minsker, *Applied Catalysis, B: Environmental*, 2012, **123-124**, 221-228.
27. H. Lan, R. Mao, Y. Tong, Y. Liu, H. Liu, X. An and R. Liu, *Environ. Sci. Technol.*, 2016, **50**, 11872-11878.
28. F. Yao, Q. Yang, M. Yan, X. Li, F. Chen, Y. Zhong, H. Yin, S. Chen, J. Fu and D. Wang, *Journal of hazardous materials*, 2020, **386**, 121651.
29. D. F. Morais, R. A. Boaventura, F. C. Moreira and V. J. Vilar, *Applied Catalysis B: Environmental*, 2019, **249**, 322-332.
30. G. S. Cunha, S. G. Santos, B. M. Souza-Chaves, T. F. Silva, J. P. Bassin, M. W. Dezotti, R. A. Boaventura, M. M. Dias, J. C. B. Lopes and V. J. Vilar, *Environmental Science and Pollution Research*, 2019, **26**, 33281-33293.
31. Y. Matatov-Meytal and M. Sheintuch, *Appl. Catal., A*, 2002, **231**, 1-16.
32. E. Joannet, C. Horny, L. Kiwi-Minsker and A. Renken, *Chemical Engineering Science*, 2002, **57**, 3453-3460.
33. M. Crespo-Quesada, R. R. Dykeman, G. Laurency, P. J. Dyson and L. Kiwi-Minsker, *Journal of Catalysis*, 2011, **279**, 66-74.
34. W. Fang, S. Yang, X.-L. Wang, T.-Q. Yuan and R.-C. Sun, *Green Chemistry*, 2017, **19**, 1794-1827.
35. P. Yaseneva, C. F. Marti, E. Palomares, X. Fan, T. Morgan, P. S. Perez, M. Ronning, F. Huang, T. Yuranova and L. Kiwi-Minsker, *Chemical Engineering Journal*, 2014, **248**, 230-241.
36. J.-W. Shim, S.-J. Park and S.-K. Ryu, *Carbon*, 2001, **39**, 1635-1642.
37. J. Rouquerol, P. Llewellyn and F. Rouquerol, *Stud. Surf. Sci. Catal.*, 2007, **160**, 49-56.
38. J. R. Anderson, *Structure of metallic catalysts*, Academic Press, London- New York, 1918.
39. A. Martinez, M. A. Arribas, M. Derewinski and A. Burkat-Dulak, *Applied Catalysis, A: General*, 2010, **379**, 188-197.
40. G. Guiler, F. Rey, J. Hernandez-Fenolosa and J. J. Cortes-Vergaz, *Journal of Physics: Conference Series*, 2013, **430**, 012057/012051-012057/012055.
41. B. Ravel and M. Newville, *Journal of Synchrotron Radiation*, 2005, **12**, 537-541.
42. E. Groppo, G. Agostini, E. Borfecchia, L. Wei, F. Giannici, G. Portale, A. Longo and C. Lamberti, *J. Phys. Chem. C*, 2014, **118**, 8406-8415.
43. E. Groppo, W. Liu, O. Zavorotynska, G. Agostini, G. Spoto, S. Bordiga, C. Lamberti and A. Zecchina, *Chem. Mater.*, 2010, **22**, 2297-2308.
44. W. J. Shen, Y. Ichihashi, H. Ando, M. Okumura, M. Haruta and Y. Matsumura, *Applied Catalysis, A: General*, 2001, **217**, 165-172.

45. A. L. Bugaev, A. A. Guda, A. Lazzarini, K. A. Lomachenko, E. Groppo, R. Pellegrini, A. Piovano, H. Emerich, A. V. Soldatov, L. A. Bugaev, V. P. Dmitriev, J. A. van Bokhoven and C. Lamberti, *Catal. Today*, 2017, **283**, 119-126.
46. M. Fernandez-Garcia, *Catalysis Reviews - Science and Engineering*, 2002, **44**, 59-121.
47. C. W. Lopes, J. L. Cerrillo, A. E. Palomares, F. Rey and G. Agostini, *Physical Chemistry Chemical Physics*, 2018, **20**, 12700-12709.
48. J. Wang, Q. Wang, X. Jiang, Z. Liu, W. Yang and A. I. Frenkel, *Journal of Physical Chemistry C*, 2015, **119**, 854-861.
49. V. V. Srabionyan, A. L. Bugaev, V. V. Pryadchenko, L. A. Avakyan, J. A. van Bokhoven and L. A. Bugaev, *Journal of Physics and Chemistry of Solids*, 2014, **75**, 470-476.
50. C. Franch, E. Rodríguez-Castellón, Á. Reyes-Carmona and A. E. Palomares, *Applied Catalysis A: General*, 2012, **425**, 145-152.
51. Z. Dong, W. Dong, F. Sun, R. Zhu and F. Ouyang, *Reaction Kinetics, Mechanisms and Catalysis*, 2012, **107**, 231-244.
52. J. Restivo, O. S. G. P. Soares, J. J. M. Orfao and M. F. R. Pereira, *Chem. Eng. J.*, 2015, **263**, 119-126.
53. M. Siddiqui, W. Zhai, G. Amy and C. Mysore, *Water Research*, 1996, **30**, 1651-1660.
54. J. Sun, J. Zhang, H. Fu, H. Wan, Y. Wan, X. Qu, Z. Xu, D. Yin and S. Zheng, *Appl. Catal., B*, 2018, **229**, 32-40.
55. W. Sun, Q. Li, S. Gao and J. K. Shang, *J. Mater. Chem. A*, 2013, **1**, 9215-9224.